Calculation of the profile-dependent neutron backscatter matrix for the JET neutron camera system

F. Binda [a],[*], G. Ericsson [a], S. Conroy [a], E. Andersson Sundén [a], JET Contributors [b][1]

[a] Department of Physics and Astronomy, Uppsala University, Uppsala, Sweden
[b] EUROfusion Consortium, JET, Culham Science Centre, Abingdon OX14 3DB, UK

HIGHLIGHTS

- Profile-dependent neutron backscatter matrices were calculated using MCNP.
- The intensity of the neutron backscatter can vary by a factor of 24
- In some cases this profile dependence of the backscatter has to be considered.

ARTICLE INFO

ABSTRACT

We investigated the dependence of the backscatter component of the neutron spectrum on the emissivity profile. We did so for the JET neutron camera system, by calculating a profile-dependent backscatter matrix for each of the 19 camera channels using a MCNP model of the JET tokamak.

We found that, when using a low minimum energy for the summation of the counts in the neutron pulse height spectrum, the backscatter contribution can depend significantly on the emissivity profile. The maximum variation in the backscatter level was 24% (8.0% when compared to the total emission). This effect needs to be considered when a correction for the backscatter contribution is applied to the measured profile.

1. Introduction

The neutron camera system at JET [1,2] provides information on the spatial distribution of the neutron emissivity of the plasma. It is composed of 19 collimated lines of sight, 10 horizontal and 9 vertical (see Fig. 1), each equipped with a NE213 liquid scintillator for the detection of DD neutrons and a BC418 plastic scintillator for DT neutrons.

The neutrons that reach the detectors can come directly from the plasma or indirectly, after scattering against the tokamak structures, the collimators or the materials surrounding the detectors. We refer to the former as "direct" and to the latter as "backscattered" neutrons, as most (but not all) of the scattered neutrons come from the tokamak wall opposite to the detector.

The proper interpretation of the neutron camera data requires a correct understanding of the backscatter component of the neutron spectrum. In previous works the intensity of the backscatter component has been considered independent of the neutron emissivity profile [1], and therefore calculated directly from the total neutron yield measurement using a constant conversion factor for each channel. The backscattered neutron energy spectrum is usually calculated, for neutron spectrometers such as TOFOR [3], from a energy-dependent backscatter matrix [4]. A first evaluation of the neutron spectrum at the detector position is multiplied with such a matrix to obtain the expected backscattered neutron spectrum.

In this study we calculated a profile-dpendent backscatter matrix for each of the neutron camera channels. We then used the matrices to evaluate the intensity of the backscatter component for different emissivity profiles.

The calculation of the backscatter matrix is presented in Section 2; the emissivity profiles used in the evaluation of the backscatter component are presented in Section 3; the steps to obtain the estimate of the camera profile measurement are pre-

* Corresponding author.
    E-mail address: federico.binda@physics.uu.se (F. Binda).
[1] See the Appendix of F. Romanelli et al., Proceedings of the 25th IAEA Fusion Energy Conference 2014, Saint Petersburg, Russia.
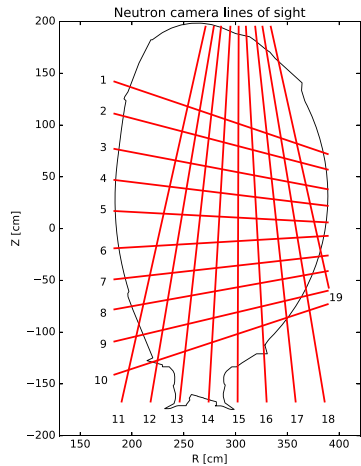
Fig. 1. Neutron camera lines of sight with corresponding reference numbers.

sented in Section 4; results and conclusions are presented in Sections 5 and 6.

2. Calculation of the backscatter matrix

The MCNP [5] model used for the calculation includes a complete geometry of the tokamak vessel and the surrounding structures (see [4] for a complete description). We used cross sections from the FENDL2.1 library.

The neutron source is uniformly sampled over a defined plasma volume, which is divided into 387 toroidal voxels ("toxels"). We ran 387 simulations, moving the source from one toxel to the other. Each toxel has a square poloidal cross section with side 10 cm. The energy distribution of the neutrons is a deuterium-deuterium reaction spectrum for a thermal plasma with temperature of 2 keV. The tallies are 19 point flux detectors located in front of each of the neutron camera scintillators, and they retain the information about the toxel of origin of the incoming neutron. Furthermore, neutrons are divided into uncollided (direct) and collided (backscattered).

For each detector of the neutron camera, the backscatter matrix is composed of the collided neutron flux spectra from each toxel. In the same way one can obtain a matrix for the direct neutrons. Fig. 2 shows the sum of the direct and backscattered neutron spectra from all toxels for detector 5. Fig. 3 shows a 2D plot of the backscatter matrix for detectors 5 and 15, after each toxel spectrum has been integrated with a neutron energy threshold of 1 MeV. It is
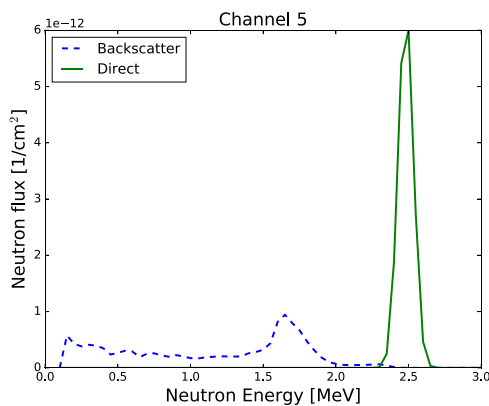

Fig. 2. Direct (solid green) and backscattered (dashed blue) neutron flux spectrum for the camera channel 5. The flux is given per JET neutron. (For interpretation of the references to color in this figure legend, the reader is referred to the web version of the article.)
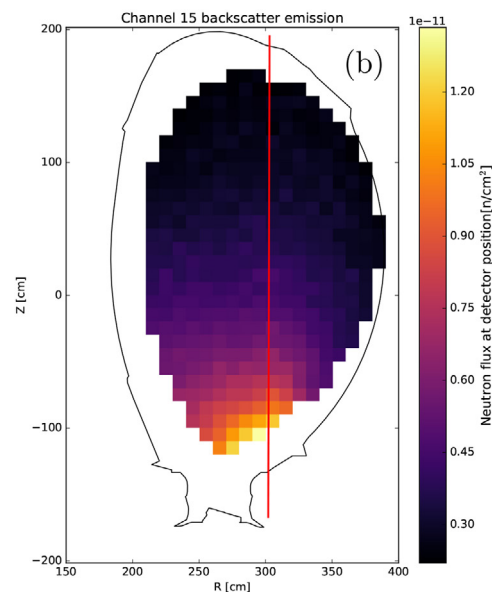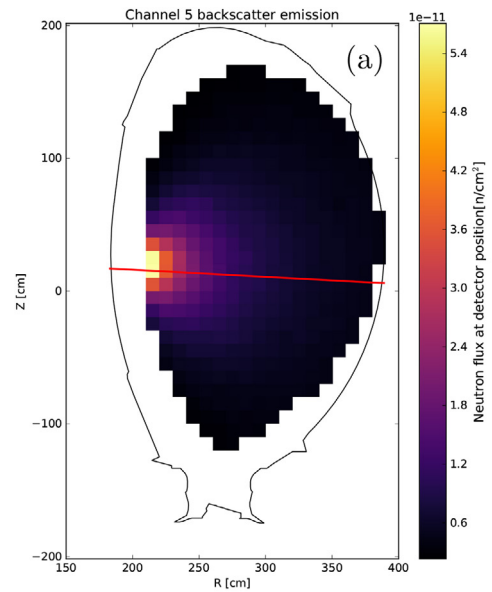

Fig. 3. Backscatter matrix for detector 5 (a) and 15 (b) after integration of the toxels with 1 MeV energy threshold. The red line shows the line of sight of the corresponding channel. (For interpretation of the references to color in this figure legend, the reader is referred to the web version of the article.)

interesting to notice how the plasma region opposite to the position of the detector is the main source for backscattered neutrons. This is because the most probable way for a neutron to scatter and then reach the detector is to scatter on the wall opposite to the detector. Neutrons generated in the plasma region close to this wall are more likely to scatter within the wall region that is seen by the detector.

3. Emissivity profiles

We studied two different types of emissivity profiles. The first is a "thermal" emissivity profile, which is given by the formula:

$$s(\rho) = S_0[(1 - \Delta)(1 - \rho)^{\alpha} + \Delta], \tag{1}$$

where S_0 is a normalization factor, Δ is a pedestal level (i.e. a base level which is constant over the entire plasma), ρ is the normalized minor radius and α is the peaking factor.
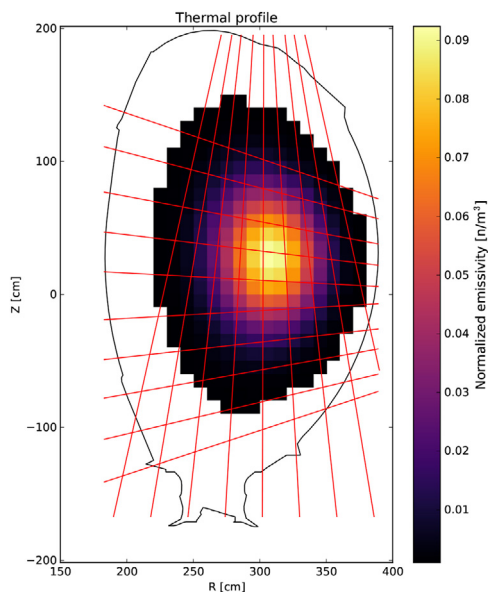
Fig. 4. Thermal emissivity profile. The camera lines of sight are superimposed.

The second is a profile for NBI heated plasmas which was given in [6]. This profile gives higher emissivity from trapped particles, and it is therefore very different from the thermal profile.

For the geometry of the magnetic surfaces, which is needed to compute the ρ values used in the calculation of the emissivity profiles, we used the constant flux surfaces given by the Flush library [7] for JET discharge number 61433 at $t = 20$ s. This is the same JET discharge and time that was used in [6] to calculate the NBI emissivity profile. The calculated thermal and NBI emissivity profiles are shown in Figs. 4 and 5 respectively.

4. Neutron camera profiles

From a given emissivity profile, the expected neutron camera profile can be obtained through the following steps:
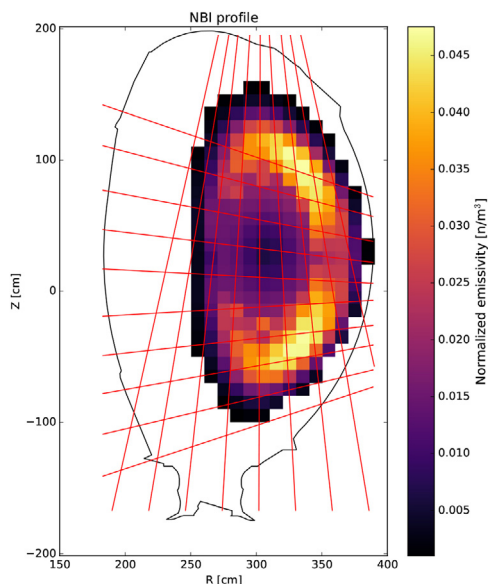

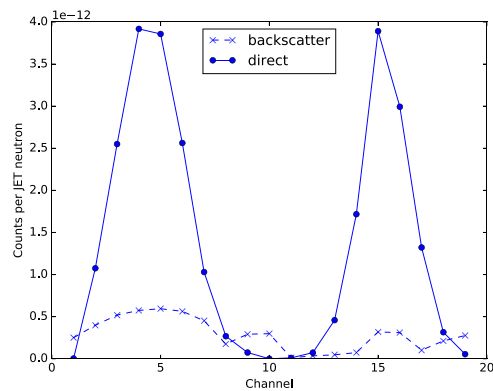Fig. 5. NBI emissivity profile. The camera lines of sight are superimposed.

Fig. 6. The neutron camera profile obtained starting from a thermal emissivity profile after integration with a 1.0 MeV neutron energy threshold.

1 multiply the emissivity profile with the backscatter and direct matrices to obtain the expected backscatter and direct neutron flux at the detector position;
2 multiply the neutron flux at the detector position with the neutron response function of the detector to obtain the backscatter and direct pulse height spectrum;
3 integrate the pulse height spectrum of each camera channel above a certain energy threshold to obtain the backscatter and direct counts which constitute the neutron camera profile as shown in Fig. 6. We give the energy threshold levels as neutron energy values; these values were converted to light yield (pulse height) threshold values for the integration of the PHS. The conversion was given by the proton light yield function from [8].

The detector response to neutrons was obtained from many MCNP simulations with a monoenergetic neutron source, each simulation with a different neutron source energy. The simulations were performed turning off the Russian roulette and using a F8 tally with a coincident F6 tally, the latter providing the conversion from proton energy to scintillation light. We took the relationship between the proton energy and the light yield from [8].

5. Results

We first investigated the camera profiles obtained from thermal emissivity profiles with different peaking factors. Fig. 7 shows the comparison of the direct and backscattered camera profiles for the two most extreme peaking factors: $\alpha = 5$ and $\alpha = 30$. The first case produces a very broad profile, the second case produces a very peaked profile. The backscattered profile however does not show relevant changes, even when a low integration energy threshold is used.

The maximum variation in backscatter level for the most important channels (2–7 and 13–17) is 3.7%. A more meaningful figure of merit can be defined as $\Delta B = (B_1 - B_2)/T_2$. where B is the backscatter profile, T is the sum of the backscatter and direct profiles, and the subscripts 1 and 2 refer to $\alpha = 5$ and $\alpha = 30$ respectively. The maximum difference that we obtain for the most important channels (2–7 and 13–17) is 0.47%. Fig. 8 shows instead the comparison between a thermal profile ($\alpha = 5$) and a "NBI" profile. In this comparison the difference in the backscatter level is clearly seen in the case of low threshold, especially for the central channels of the horizontal camera (3–6). The maximum variation in backscatter level in this case is 24%. If we instead quantify the difference using the better figure of merit, with the subscript 2 referring to the NBI profile, the maximum difference for the most important channels is 8.0%.
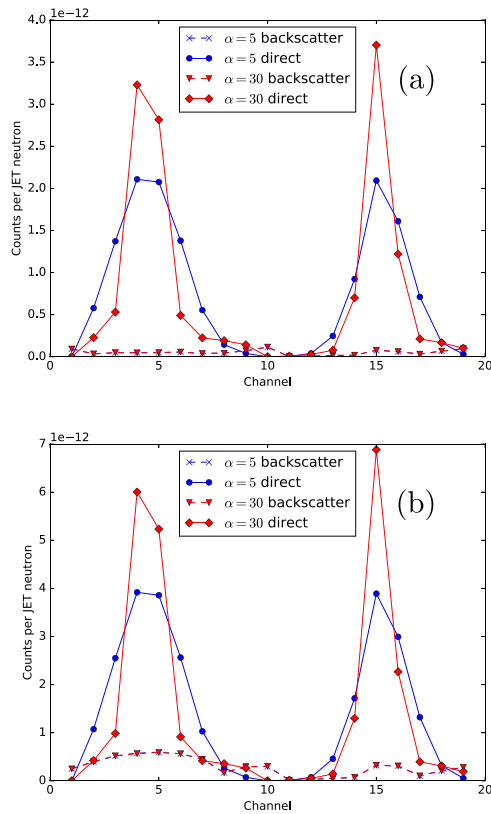
Fig. 7. The calculated camera profile for a $\alpha = 5$ and a $\alpha = 30$ thermal emissivity profile. In panel (a) the energy threshold for the integration was 1.8 MeV, in panel (b) the threshold was 1.0 MeV.
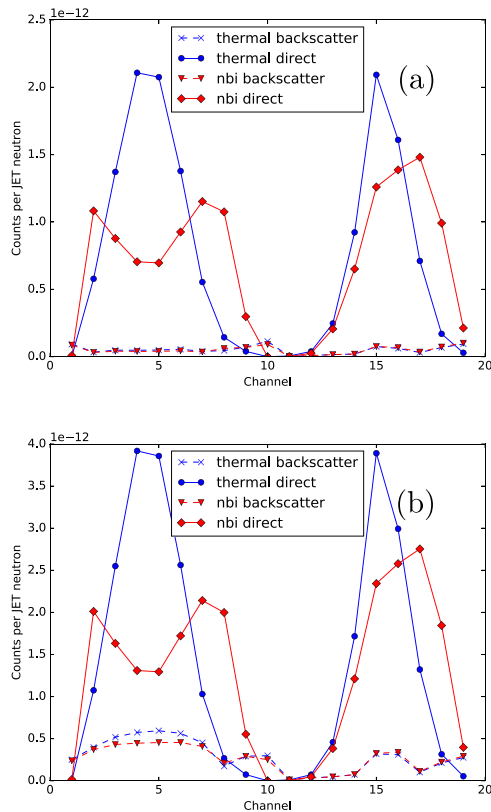
Fig. 8. The calculated camera profile for a thermal ($\alpha = 5$) and an NBI emissivity profile. In panel (a) the energy threshold for the integration was 1.8 MeV, in panel (b) the threshold was 1.0 MeV.

6. Conclusions

We calculated a profile-dependent neutron backscatter matrix for the JET neutron camera using a MCNP model. We then applied it to evaluate the dependence of the backscatter contribution on the emissivity profile. The backscatter contribution to the profile measurement can be considered independent of the emissivity profile only if the integration threshold is high enough (1.8 MeV). For lower thresholds the backscatter contribution does depend on the emissivity profile. In the most extreme case the difference in the backscatter level was 24%, or 8.0% if compared to the total emission. This effect should be considered in the analysis of experimental data.

Acknowledgments

References

[1] J.M. Adams, et al., The JET neutron emission profile monitor, Nucl. Instrum. Methods Phys. Res. A 329 (1993) 277–290, http://dx.doi.org/10.1016/0168-9002(93)90947-G.

[2] M. Riva, et al., The new digital electronics for the JET neutron profile monitor: Performances and first experimental results, Fusion Eng. Des. 86 (2011) 1191–1195, http://dx.doi.org/10.1016/j.fusengdes.2011.02.038.

[3] M. Gatu Johnson, et al., The 2.5-MeV neutron time-of-flight spectrometer TOFOR for experiments at JET, Nucl. Instrum. Methods Phys. Res. A 591 (2008) 417–430, http://dx.doi.org/10.1016/j.nima.2008.03.010.

[4] M.G. Johnson, et al., Modelling and TOFOR measurements of scattered neutrons at JET, Plasma Phys. Control. Fusion 52 (2010) 085002, http://dx.doi.org/10.1088/0741-3335/52/8/085002.

[5] J.T. Goorley, et al., Initial MCNP6 release overview-MCNP6 version 1.0, in: Tech. Rep. LA-UR-13-22934, Los Alamos National Laboratory (LANL), 2013 http://permalink.lanl.gov/object/tr?what=info:lanl-repo/lareport/LA-UR-13-22934.

[6] E. Ronchi, et al., A parametric model for fusion neutron emissivity tomography for the KN3 neutron camera at JET, Nucl. Fusion 50 (2010) 035008, http://dx.doi.org/10.1088/0029-5515/50/3/035008.

[7] A. Pamela, FLUSH User's Guide, UKAEA, JET document, 2nd ed., 2013, September http://users.euro-fusion.org/pages/data-proc/flush/flush_manual.pdf.

[8] N.P. Hawkes, et al., Measurements of the proton light output function of the organic liquid scintillator NE213 in several detectors, Nucl. Instrum. Methods Phys. Res. A 476 (2002) 190–194, http://dx.doi.org/10.1016/S0168-9002(01)01429-2.